Combination of Molecular, Morphological, and Interfacial Engineering to Achieve Highly Efficient and Stable Plastic Solar Cells

Chih-Yu Chang, Yen-Ju Cheng, Shih-Hsiu Hung, Jhong-Sian Wu, Wei-Shun Kao, Chia-Hao Lee, and Chain-Shu Hsu**

Flexible photovoltaics that are conformationally adjustable according to the shape of the substrate have attracted much industrial and academic research interest.[1] Polymer solar cells (PSCs) are the most suitable for rollable and bendable cells because organic-based photoactive materials can be coated or printed on lightweight plastic foil to achieve excellent conformal flexibility.[2–4] One of the appealing applications of flexible cells is to integrate them in textile products to power portable electronic devices with lower energy demand. Before flexible PSCs can be smartly utilized in multifunctional applications, significant progress must be made in improving power conversion efficiency (PCE), long-term stability in the presence of moisture and oxygen, and stable performance despite mechanical deformation.[3–5] The most formidable challenges in making highly efficient PSCs are to simultaneously optimize three interconnected parameters by 1) development of photoactive materials with superior molecular properties,[5–8] 2) manipulation of material processing to control active layer morphology,[9–11] and 3) improvement of interface characteristics by advanced device engineering.[11–13] The tricyclic 2,7-fluorene unit has proved to be a superb electron-rich building block for constructing donor–acceptor (D–A) polymers because its derivatives have been shown to have deep-lying highest occupied molecular orbital (HOMO) energy levels and good hole-transporting properties, which are crucial prerequisites to achieving high open-circuit voltages (V_{oc}) and short-circuit currents (J_{sc}), respectively.[7,14] The alternating copolymer poly(2,7-fluorene-*alt*-dithienylbenzothiadiazole) (PFDTBT) has proved to be a promising class of p-type photoactive material for application in PSCs.[15] Considering that forced planarization by covalently fastening adjacent aromatic units in polymer backbone facilitates π-electron delocalization to narrow the bandgap and suppresses the interannular rotation to enhance intrinsic charge mobility,[7,16–18] we recently reported a PFDTBT-based analogue, poly(fluorenedicyclopentathiophene-*alt*-benzothiadiazole) (PFDCTBT),[19] where the 3-positions of two outer thiophenes are covalently tied with the 3,6-positions of the central fluorene core by a carbon bridge (**Figure 1**). The four 4-(2-ethylhexoxy)-phenyl groups introduced to the fluorenedicyclopentathiophene (FDCT) structure promote the solubility and processing capability of the resulting polymer. However, the branch and rigid ethylhexoxyphenyl groups sticking out of the coplanar backbone of FDCT may in turn suppress the intermolecular interaction. Consequently, the solar cell device based on the blend of PFDCTBT: [6,6] phenyl-C_{71}-butyric acid methyl ester ($PC_{71}BM$) delivered only a moderate PCE of 2.8%.[19] It is envisaged that modification of the molecular structure of FDCT by replacing the branch ethylhexoxyphenyl groups by more flexible aliphatic groups could tailor the intermolecular interaction to optimize bulk properties such as enhanced absorption intensity, reduced optical bandgap, and improved charge mobility.[20,21] However, introduction of aliphatic side chains into fused arenes by means of an intramolecular Friedel–Crafts alkylation approach is synthetically challenging owing to a competing elimination reaction.[21] To overcome this difficulty, we employed a three-step acylation–reduction–alkylation strategy to successfully synthesize a new PFDCTBT-C8 copolymer consisting of octyl side chains on the cyclopentadienyl rings (Figure 1).

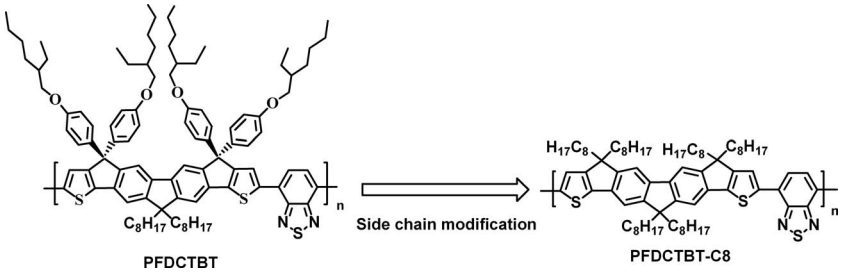

Figure 1. Chemical structures of PFDCTBT and PFDCTBT-C8 with octyl side chains.

The synthesis of the key Br-FDCT-C8 monomer leading to PFDCTBT-C8 is shown in **Scheme 1**. Compound **1** with two ester groups was hydrolyzed to form compound **2** with two carboxylic acids, which were then converted to acid chlorides by reacting with oxayl chloride to afford intermediate **3**. Intramolecular Friedel–Crafts acylation of **3** regioselectively occurred at the 3- and 6-positions of the central flourene to yield the heptacyclic arene **4**. Wolff–Kishner reduction converted the two carbonyl groups in compound **4** to the corresponding methylene

Dr. C.-Y. Chang, Prof. Dr. Y.-J. Cheng, S.-H. Hung, J.-S. Wu, W.-S. Kao, C.-H. Lee, Prof. Dr. C.-S. Hsu
Department of Applied Chemistry
National Chiao Tung University
1001 Ta Hseuh Road, Hsin-Chu 30010, Taiwan, R.O.C.
E-mail: yjcheng@mail.nctu.edu.tw;
cshsu@mail.nctu.edu.tw

DOI: 10.1002/adma.201103945

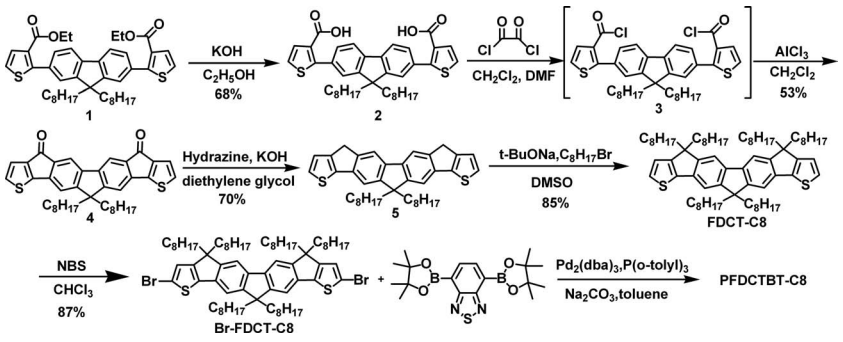

Scheme 1. Synthesis of Br-FDCT-C8 monomer and PFDCTBT-C8 copolymer.

groups in compound **5**. Alkylation of compound **5** successfully incorporated four octyl groups in FDCT-C8, which was then brominated by *N*-bromosuccinimide (NBS) to afford Br-FDCT-C8. This monomer was copolymerized with the 4,7-bis(4,4,5,5-tetramethyl-1,3,2-dioxaborolan-2-yl)-2,1,3-benzothiadiazole (BT) unit by Suzuki coupling to generate the D–A copolymer PFDCTBT-C8, which showed a number-average molecular weight (M_n) of ca. 33 kDa with a polydispersity index of 2.87, as determined by gel permeation chromatography.

From thermal gravimetric analysis (TGA), we found PFDCTBT-C8 had high thermal stability with a decomposition temperature (5% weight loss) of 437 °C (Figure S1, Supporting Information). The UV-vis absorption spectra of PFDCTBT-C8 in toluene showed two distinct absorption bands (**Figure 2**). The short-wavelength absorption band (ca. 417 nm) is assigned to a delocalized excitonic π–π^* transition and the long-wavelength absorption band (ca. 621 nm) is ascribed to intramolecular charge transfer (ICT) interactions between the donor and acceptor moieties. It should be noted that the profiles of the absorption spectra of PFDCTBT are essentially the same in both the solution state and the solid state (Figure 2), indicating that the bulky 4-(2-ethylhexyloxy)phenyl moieties in PFDCTBT dilute the interchain π–π interactions in the solid state. Nevertheless, the absorption maxima of PFDCTBT-C8, substituted with flexible octyl side chains, red-shifted by ca. 20 nm from the toluene solution to the solid state (Figure 2). Furthermore, the optical bandgap of PFDCTBT-C8 deduced from its absorption edge in the solid state was determined to be 1.71 eV, which is narrower than that of PFDCTBT (1.76 eV). These optical behaviors confirm that the side chain modification of PFDCTBT-C8 effectively promotes stronger intermolecular interaction in the solid state.

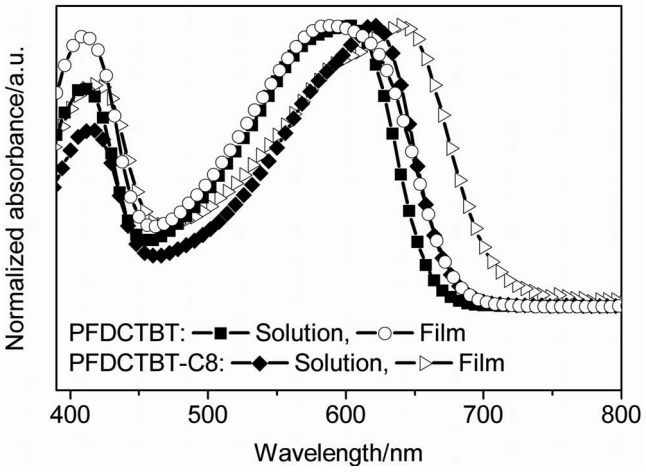

Figure 2. UV–vis absorption spectra of PFDCTBT and PFDCTBT-C8 in toluene solution and in the film state.

The electrochemical properties of PFDCTBT-C8 were estimated by cyclic voltammetry (CV) (Figure S2). The flourene-based PFDCTBT-C8 showed a typical lower-lying HOMO level at –5.30 eV, which is an important criterion for obtaining high V_{oc} in the resultant device.[3,4] The lowest unoccupied molecular orbital (LUMO) level of PFDCTBT-C8 was determined to be –3.55 eV, that is, positioned 0.4 eV above that of electron acceptor $PC_{71}BM$ (–3.95 eV, measured under the same conditions), which will ensure energetically favorable electron transfer.[3,4]

The field-effect hole mobilities of PFDCTBT and PFDCTBT-C8 were extracted from the transfer characteristics of the field-effect transistor (FET) devices fabricated with top-contact geometry using Au electrodes (**Figure 3**a). PFDCTBT-C8 exhibited a high field-effect hole mobility of 3.3×10^{-2} cm^2 V^{-1} s^{-1} owing to the extended coplanarity and rigidity of FDCT's structure. It should be noted that this value is higher than that of PFDCTBT (1.4×10^{-3} cm^2 V^{-1} s^{-1}) by an order of magnitude. This result indicates that flexible aliphatic side chains in PFDCTBT-C8 strengthen the intermolecular π–π interaction to enhance the hole mobility compared to the ethylhexoxyphenyl side chains in PFDCTBT.

The solar cells with inverted architecture were fabricated based on the configuration indium tin oxide (ITO)/ZnO/C-PCBSD/PFDCTBT-C8:$PC_{71}BM$ (1:3, w/w)/poly(3,4-ethylenedioxythiophene) poly(styrenesulfonate) (PEDOT:PSS)/Ag where a cross-linked $PC_{61}BM$ derivative, [6,6]-phenyl-C_{61}-butyric styryl dendron ester (C-PCBSD), was used as an interlayer.[22–24] Current density–voltage (*J*–*V*) characteristics of the devices under AM1.5G solar irradiation with light intensity of 100 mW cm^{-2} are shown in Figure 3b, and the corresponding device parameters are summarized in **Table 1**. When the active layer was processed with only *ortho*-dichlorobenzene (ODCB) as the solvent, device A obtained a high PCE of 4.8% with V_{oc} of 0.83 V, J_{sc} of 10.35 mA cm^{-2}, and fill factor (FF) of 55.7% (Table 1 and Figure 3b). The nanometer-scale morphology of the active layer can be smartly controlled by judicial choice of the processing additives.[10,11,25] Encouragingly, by adding 2.5 vol.% 1-chloronaphthalene (CN) into ODCB as the processing additive in device B, the PCE was dramatically improved to 6.7% as a result of the simultaneously increased J_{sc} and FF values (Table 1 and Figure 3b). Note that the J_{sc} values from *J*–*V* measurements are consistent with the values calculated from integrated incident photon–to–current conversion efficiency (IPCE) spectra (Figure S3), which confirms the accuracy of the reported PCE values.

To gain deep insight into the performance enhancement upon the introduction of CN additive, the morphological alteration of the blend films was investigated by atomic force microscopy (AFM) topography images (Figure S4). Compared to the

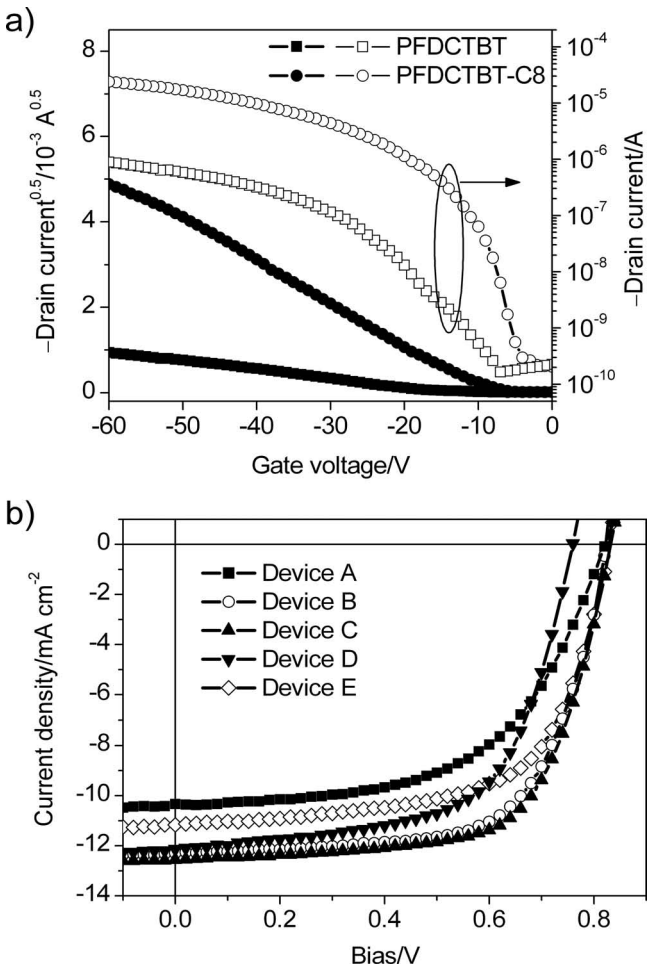

Figure 3. a) Transfer characteristics (V_{ds} = –60 V) of the FET devices based on PFDCTBT and PFDCTBT-C8 thin films. b) Current density–voltage (*J–V*) characteristics of the as-fabricated solar cell devices A–E; see Table 1 for descriptions of the device types.

pristine film, the additive-processed PFDCTBT-C8:$PC_{71}BM$ film showed more pronounced fiber-like nanostructures with greater surface roughness. To further understand the effect of the additive on the device performance, electron- and hole-only devices were fabricated to estimate the charge mobilities of the blend films by a space charge limited current (SCLC) model;[26,27] the results are shown in Table 1 and Figure S5. The additive-processed device exhibited a hole mobility increased by almost one order of magnitude (from 1.3×10^{-4} cm^2 V^{-1} s^{-1} to 9.8×10^{-4} cm^2 V^{-1} s^{-1}) while the electron mobilities of the devices remained essentially unchanged (ca. 9.4×10^{-4} cm^2 V^{-1} s^{-1}). In addition to the enhancement in SCLC hole mobility, the field-effect hole mobility of PFDCTBT-C8 was also increased from 3.3×10^{-2} cm^2 V^{-1} s^{-1} to 8.9×10^{-2} cm^2 V^{-1} s^{-1} by adding 2.5 vol% CN as the processing additive (Figure S6). In view of optimized morphology and enhanced hole mobility, we assume that the performance enhancement is attributed to the additive-assisted self-organization of PFDCTBT-C8 into a more favorable morphology that facilitates hole transporting properties. The more balanced electron/hole mobilities (the electron-to-hole mobility ratio is close to unity) can effectively reduce space charge build-up within the active layer.[9,27]

Based on the optimized molecular and morphological properties, we envision that modulating interface characteristics between PEDOT:PSS layer and anode may play an important role in further improvement of inverted device performance.[11,13] By inserting a solution-processed vanadium oxide (VO_x) film on top of the PEDOT:PSS layer in device C,[28,29] we successfully achieved an exceptionally high PCE of 7%, which represents the highest value ever reported for fluorine-based bulk-heterojunction (BHJ) solar cells (Table 1, Figure 3b). Device C also exhibited a higher shunt resistance, of 5.8 MΩ cm^2, than device B, with 0.7 MΩ cm^2 (Figure S7), indicating that the leakage current in device B can be greatly suppressed by the VO_x layer in device C. This result might be associated with the passivation of the local shunts existing within the PEDOT:PSS layer.[30,31] However, device D, using VO_x as the single hole-extraction layer (without PEDOT:PSS layer), exhibited a PCE reduced to 5.7%. This decrease obviously originated from the decreased V_{oc} (Table 1 and Figure 3b). The mechanism of the V_{oc} reduction in device D is not clear, but it may arise from the poor electrical coherence at the organic/inorganic interface and/or trap formation as a result of the penetration of the vanadium precursor into the active layer.[32–34] Further investigation is currently under way in our laboratory.

In addition, the shelf-stability of devices B and C without encapsulation was evaluated by monitoring the evolution of their PCE as a function of time during storage under ambient conditions. (**Figure 4**a). In contrast to device B, which showed a more obvious decline, device C retained over 85% of its initial PCE after being exposed to ambient conditions for more than 690 h, suggesting that the VO_x interlayer may act as a gas-permeation barrier that prevents ambient H_2O/O_2 from degrading the underlying organic materials.[35] PEDOT:PSS is known for

Table 1. Summary of the parameters based on the devices substrate/ITO/ZnO/C-PCBSD/PFDCTBT-C8:$PC_{71}BM$ (1:3, w/w)/HEL/Ag.

Device	Conditions[a)]	V_{oc} [V]	J_{sc} [mA cm^{-2}]	FF [%]	PCE [%]	Hole mobility[c)] [cm^2 V^{-1} s^{-1}]	Electron mobility[c)] [cm^2 V^{-1} s^{-1}]
A	Glass, without, PEDOT:PSS	0.83	10.35 (9.81)[b)]	55.7	4.8	1.3×10^{-4}	9.8×10^{-4}
B	Glass, with, PEDOT:PSS	0.83	12.29 (11.97)[b)]	65.6	6.7	9.3×10^{-4}	9.4×10^{-4}
C	Glass, with, PEDOT:PSS + VO_x	0.83	12.57 (12.35)[b)]	66.8	7.0	-	-
D	Glass, with, VO_x	0.76	12.14	61.9	5.7	-	-
E	Plastic, with, PEDOT:PSS + VO_x	0.83	11.31 (10.44)[b)]	63.4	6.0	-	-

[a)]Substrate, with or without CN additive, hole-extraction layer (HEL); [b)]Calculated from the IPCE spectra shown in Figure S3 (Supporting Information); [c)]Estimated by SCLC model.

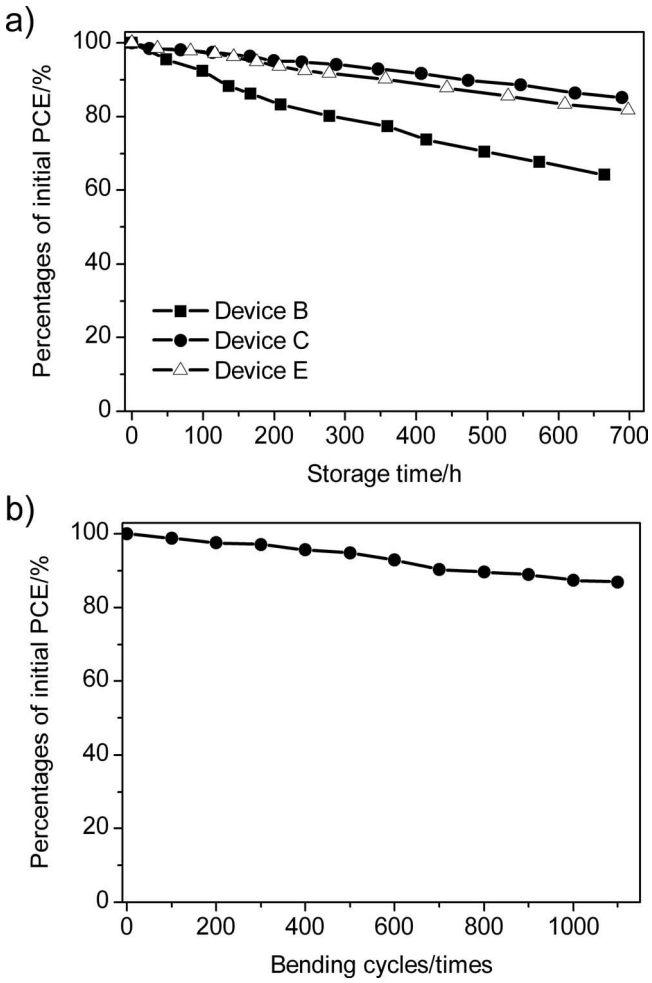

Figure 4. a) Degradation profiles of the unencapsulated devices B, C, and E stored at 30 °C in ambient air. b) The PCE degradation profile of flexible device E during consecutive bending cycles with a radius of 12 mm.

its acidity, which could result in erosion or passivation of the adjacent electrode. Avoiding direct contact between PEDOT:PSS and the Ag electrode by inserting a VO_x interlayer might also be a possible reason for the improved long-term stability.

To truly exploit flexibility of PSCs for practical use, multilayer devices have to be integrated with a plastic substrate. However, plastic-based solar cells still suffer from insufficient efficiency and poor stability compared to their glass-based counterparts.[5] So far, the realization of plastic solar cells with PCE values above 5% has not been successful.[36] It is highly desirable to transfer our optimal device configuration from a glass substrate to a plastic substrate. By taking advantage of the fact that all the device fabrication processing conditions in this research were at low temperatures below 150 °C, we successfully fabricated device E on ITO-coated poly(ethylene naphthalate) (PEN) substrate. As shown in Table 1 and Figure 3b, device E exhibited an exceptional PCE of 6%, with V_{oc} of 0.83 V, J_{sc} of 11.31 mA cm^{-2}, and FF of 63.4%. The lower efficiency observed in device E relative to device C is due to intrinsic limitations of the PEN plastic substrate, including the higher ITO sheet resistance (50 Ω sq^{-1} vs. 15 Ω sq^{-1} on the glass substrate) and lower optical transparency (Figure S8). Again, device E also exhibited excellent air stability, retaining over 80% of its initial PCE after being exposed to ambient conditions for more than 690 h (Figure 4a).

Device stability with respect to mechanical deformation is another important device parameter for flexible solar cells. To evaluate the mechanical stability under ambient conditions, planar device E was first bent to a circle with a radius of 12 mm followed by recovery to planar structure. After 1100 bending cycles in which an external force was consecutively applied and released, device E showed no significant decrease of efficiency, maintaining 87% of its original PCE (Figure 4b). This result demonstrated that device E possesses good flexibility without compromising its high device performance. The superior mechanical stability might be associated with the small thickness of the metal oxide layers (i.e., 20 nm ZnO and 15 nm VO_x) used in the device to avoid crack formation during the bending process.

In conclusion, by an acylation–reduction–alkylation strategy we have successfully synthesized a novel fluorine-based multifused D–A alternating copolymer PFDCTBT-C8 substituted with flexible octyl groups. PFDCTBT-C8 features a narrow bandgap of 1.71 eV, a low-lying HOMO level of –5.30 eV, and a high field-effect hole mobility of 3.3×10^{-2} cm^2 V^{-1} s^{-1}. Through engineering molecular structure to promote the intermolecular interaction, using additive to assist the formation of the optimized morphology, and introducing a VO_x interlayer to improve the interfacial properties, we achieved a BHJ solar cell based on PFDCTBT-C8:$PC_{71}BM$ (1:3, w/w) blend with an impressive PCE of 7%, which represents the highest value ever reported for fluorine-based BHJ solar cells. More significantly, the device constructed on the flexible PEN substrate not only achieved a record high PCE of 6% for plastic solar cells, but also exhibited exceptional air and mechanical stability.

Experimental Section

PSC Device Fabrication and Characterization: The device structure of the solar cell device was substrate/ITO/ZnO/C-PCBSD/PFDCTBT-C8:$PC_{71}BM$/PEDOT:PSS/with or without VO_x/Ag. Substrates included ITO-coated glass (purchased from Rite Displays; sheet resistance 15 Ω sq^{-1}) and ITO-coated PEN (purchased from Perm Top Corp.; sheet resistance 50 Ω sq^{-1}). The device fabrication procedure was described as follows: 1) spin casting of the ZnO precursor from zinc acetylacetonate hydrate (purchased from Aldrich and used as received) dissolved in methanol (20 mg mL^{-1}) onto the pre-cleaned ITO surface and subsequent baking at 130 °C for 10 min in air (20 nm); 2) spin casting of PCBSD solution (7 mg mL^{-1} in ODCB) on top of the ZnO layer (ca. 10 nm) and subsequent baking at 150 °C for 10 min; 3) spin casting of the active layer (150 nm) from an ODCB solution of PFDCTBT-C8 (6 mg mL^{-1}) and $PC_{71}BM$ (18 mg mL^{-1}, purchased from Solenne and used as received); 4) spin casting of the PEDOT:PSS layer (Clevios P from Heraeus Clevios) diluted with an equal volume of 2-propanol and 0.2 wt% polyoxyethylene-6-tridecylether (Aldrich) followed by baking at 60 °C for 10 min (60 nm); 5) spin casting of the VO_x layer (15 nm) from the isopropyl alcohol solution of vanadium(V) triisopropoxy (purchased from Alfa Aesar and used as received) at 1:70 volume ratio for the device containing the VO_x layer;[28] 6) thermal evaporation of the Ag layer under high vacuum (<10^{-6} Torr; 200 nm) through a shadow mask that defined an active area of 0.04 cm^2; 7) thermal annealing of the complete device at 150 °C for 5 min. The *J–V* characteristics of the PSC devices

were measured with a Keithley 2400 source meter under simulated AM1.5G illumination (SAN-EI XES-301S solar simulator with integrated intensity of 100 mW cm^{-2}), which was calibrated with a Hamamatsu silicon photodiode with KG-5 filter against an NREL-calibrated solar simulator.[37] IPCE spectra were measured using a lock-in amplifier with a current preamplifier under short-circuit conditions with illumination by monochromatic light from a 250 W quartz-halogen lamp (Osram) passing through a monochromator (Spectral Products CM110).

FET Device Fabrication and Characterization: Top-contact, bottom-gate FET devices were fabricated on heavily doped n-type Si wafer substrates with thermally grown SiO_2 gate dielectric (300 nm, capacitance 10 nF cm^{-2}).[38] The cleaned substrates were immersed in a 0.1 M solution of octadecyltrichlorosilane (OTS) in toluene at 60 °C for 3 h under an inert atmosphere followed by rinsing with toluene and then drying with N_2. The PFDCTBT and PFDCTBT-C8 solutions (7 mg mL^{-1} in ODCB) were then deposited on top of the OTS-modified SiO_2 surface followed by baking at 150 °C for 5 min. Subsequently, the Au source/drain electrodes were deposited by thermal evaporation through a shadow mask to finish the FET devices with channel length L and channel width W of 60 μm and 3500 μm, respectively. Electrical characterization was carried out under vacuum using an Agilent 4156C semiconductor parameter analyzer. The FET mobility was extracted from the following equation in the saturation regime: $I_D = \mu C_i (W/2L)(V_G - V_T)^2$,[38] where I_D is the drain current, W and L are the channel width and length, respectively, C_i is the capacitance per unit area of the gate dielectric, and V_G is the gate voltage.

Supporting Information

Supporting Information is available from the Wiley Online Library or from the author.

Acknowledgements

This work is supported by the National Science Council and "ATP Plan" of the National Chiao Tung University and Ministry of Education, Taiwan.

Received: October 13, 2011
Published online: December 20, 2011

[1] M. Pagliaro, R. Ciriminna, G. Palmisano, *ChemSusChem* **2008**, *1*, 880.
[2] G. Yu, J. Gao, J. C. Hummelen, F. Wudl, A. J. Heeger, *Science* **1995**, *270*, 1789.
[3] K. M. Coakley, M. D. McGehee, *Chem. Mater.* **2004**, *16*, 4533.
[4] B. C. Thompson, J. M. J. Fréchet, *Angew. Chem. Int. Ed.* **2008**, *47*, 58.
[5] C. J. Brabec, S. Gowrisanker, J. J. M. Halls, D. Laird, S. Jia, S. P. Williams, *Adv. Mater.* **2010**, *22*, 3839.
[6] Y. Li, Y. Zou, *Adv. Mater.* **2008**, *20*, 2952.
[7] Y. J. Cheng, S. H. Yang, C. S. Hsu, *Chem. Rev.* **2009**, *109*, 5868.
[8] C. A. Junwu, C. Yong, *Acc. Chem. Res.* **2009**, *42*, 1709.
[9] G. Li, V. Shrotriya, J. Huang, Y. Yao, T. Moriarty, K. Emery, Y. Yang, *Nat. Mater.* **2005**, *4*, 864.
[10] J. Peet, J. Y. Kim, N. E. Coates, W. L. Ma, D. Moses, A. J. Heeger, G. C. Bazan, *Nat. Mater.* **2007**, *6*, 497.
[11] L. M. Chen, Z. Hong, G. Li, Y. Yang, *Adv. Mater.* **2009**, *21*, 1434.
[12] M. D. Irwin, D. B. Buchholz, A. W. Hains, R. P. H. Chang, T. J. Marks, *Proc. Natl. Acad. Sci. USA* **2008**, *105*, 2783.
[13] H. Ma, H.-L. Yip, F. Huang, A. K. Y. Jen, *Adv. Funct. Mater.* **2010**, *20*, 1371.
[14] F. Zhang, W. Mammo, L. M. Andersson, S. Admassie, M. R. Andersson, O. Inganäs, *Adv. Mater.* **2006**, *18*, 2169.
[15] M. H. Chen, J. Hou, Z. Hong, G. Yang, S. Sista, L. M. Chen, Y. Yang, *Adv. Mater.* **2009**, *21*, 4238.
[16] W. Wu, Y. Liu, D. Zhu, *Chem. Soc. Rev.* **2010**, *39*, 1489.
[17] M. Forster, K. O. Annan, U. Scherf, *Macromolecules* **1999**, *32*, 3159.
[18] M. Forster, J. Y. Pan, K. O. Annan, D. Haarer, U. Scherf, *Polym. Int.* **2000**, *49*, 913.
[19] J. S. Wu, Y. J. Cheng, M. Dubosc, C. H. Hsieh, C. Y. Chang, C. S. Hsu, *Chem. Commun.* **2010**, *46*, 3259.
[20] M. Zhang, X. Guo, X. Wang, H. Wang, Y. Li, *Chem. Mater.* **2011**, *23*, 4264.
[21] Y. J. Cheng, J. S. Wu, P. I. Shih, C. Y. Chang, P. C. Jwo, W. S. Kao, C. S. Hsu, *Chem. Mater.* **2011**, *23*, 2361.
[22] C. H. Hsieh, Y. J. Cheng, P. J. Li, C. H. Chen, M. Dubosc, R. M. Liang, C. S. Hsu, *J. Am. Chem. Soc.* **2010**, *132*, 4887.
[23] Y.-J. Cheng, C.-H. Hsieh, Y. He, C.-S. Hsu, Y. Li, *J. Am. Chem. Soc.* **2010**, *132*, 17381.
[24] C.-Y. Chang, C.-E. Wu, S.-Y. Chen, C. Cui, Y.-J. Cheng, C.-S. Hsu, Y.-L. Wang, Y. Li, *Angew. Chem. Int. Ed.* **2011**, *50*, 9386.
[25] C. V. Hoven, X. D. Dang, R. C. Coffin, J. Peet, T. Q. Nguyen, G. C. Bazan, *Adv. Mater.* **2010**, *22*, E63.
[26] M. F. Falzon, M. M. Wienk, R. A. J. Janssen, *J. Phys. Chem. C* **2011**, *115*, 3178.
[27] V. D. Mihailetchi, H. Xie, B. De Boer, L. J. A. Koster, P. W. M. Blom, *Adv. Funct. Mater.* **2006**, *16*, 699.
[28] K. Zilberberg, S. Trost, H. Schmidt, T. Riedl, *Adv. Energy Mater.* **2011**, *1*, 377.
[29] C. P. Chen, Y. D. Chen, S. C. Chuang, *Adv. Mater.* **2011**, *23*, 3859.
[30] A. W. Hains, T. J. Marks, *Appl. Phys. Lett.* **2008**, *92*, 0235041.
[31] M. Kemerink, S. Timpanaro, M. M. de Kok, E. A. Meulenkamp, F. J. Touwslager, *J. Phys. Chem. B* **2004**, *108*, 18820.
[32] C. Goh, S. R. Scully, M. D. McGehee, *J. Appl. Phys.* **2007**, *101*, 114503.
[33] K. Zilberberg, S. Trost, J. Meyer, A. Kahn, A. Behrendt, D. Lützenkirchen-Hecht, R. Frahm, T. Riedl, *Adv. Funct. Mater.* doi: 10.1002/adfm.201101402.
[34] S. R. Cowan, W. L. Leong, N. Banerji, G. Dennler, A. J. Heeger, *Adv. Funct. Mater.* **2011**, *21*, 3083.
[35] H. Hintz, H. J. Egelhaaf, L. Lüer, J. Hauch, H. Peisert, T. Chassé, *Chem. Mater.* **2011**, *23*, 145.
[36] J.-C. Wang, W.-T. Weng, M.-Y. Tsai, M.-K. Lee, S.-F. Horng, T.-P. Perng, C.-C. Kei, C.-C. Yu, H.-F. Meng, *J. Mater. Chem.* **2010**, *20*, 862.
[37] V. Shrotriya, G. Li, Y. Yao, T. Moriarty, K. Emery, Y. Yang, *Adv. Funct. Mater.* **2006**, *16*, 2016.
[38] J. H. Oh, H. W. Lee, S. Mannsfeld, R. M. Stoltenberg, E. Jung, Y. W. Jin, J. M. Kim, J. B. Yoo, Z. Bao, *Proc. Natl. Acad. Sci. USA* **2009**, *106*, 6065.